Intraoperative Brain Resection Cavity Characterization with Conoscopic Holography

Amber L. Simpson[a], Jessica Burgner[b], Ishita Chen[a], Thomas S. Pheiffer[a], Kay Sun[a],
Reid C. Thompson[c], Robert J. Webster III[b], and Michael I. Miga[a]

[a] Department of Biomedical Engineering, Vanderbilt University, Nashville, Tennessee, USA
[b] Department of Mechanical Engineering, Vanderbilt University, Nashville, Tennessee, USA
[c] Department of Neurological Surgery, Vanderbilt University, Nashville, Tennessee, USA

ABSTRACT

Brain shift compromises the accuracy of neurosurgical image-guided interventions if not corrected by either intraoperative imaging or computational modeling. The latter requires intraoperative sparse measurements for constraining and driving model-based compensation strategies. Conoscopic holography, an interferometric technique that measures the distance and direction of a laser light illuminated surface point from a fixed laser source, was recently proposed for non-contact surface data acquisition in image-guided surgery and is used here for validation of our modeling strategies.

In this contribution, we use this inexpensive, hand-held conoscopic holography device for intraoperative validation of our computation modeling approach to correcting for brain shift. Laser range scan, instrument swabbing, and conoscopic holography data sets were collected from two patients undergoing brain tumor resection therapy at Vanderbilt University Medical Center. The results of our study indicate that conoscopic holography is a promising method for surface acquisition since it requires no contact with delicate tissues and can characterize the extents of structures within confined spaces. We demonstrate that for two clinical cases, the acquired conoprobe points align with our model-updated images better than the uncorrected ones lending further evidence that computation modeling approaches improve the accuracy of image-guided surgical interventions in the presence of soft tissue deformations.

1. INTRODUCTION

The success of an image-guided surgical intervention is contingent on the determination of the spatial relationship between the preoperative patient images and the intraoperative state of the patient in the operating theater. In neurosurgery, this relationship is compromised by brain tissue deformation and shift that occurs during resection. The nature and extent of the shift is dependent on factors such as gravity, edema, hyperosnotic drugs, the nature of the pathology, and the resection process itself.[1–3] In the course of an intervention, the brain can deform over a centimeter in a non-uniform way.[4] There are two primary methods of compensating for brain shift: intraoperative imaging[5–7] and computation modeling techniques for correcting the guidance display.[8–12] In the case of the latter, the intraoperative validation of these models is a challenging problem. In this paper, we investigate the use of conoscopic holography for the characterization of the resection cavity in two *in vivo* cases toward an intraoperative validation framework for deformation correction schemes that use sophisticated mathematical models.

Many authors describe the application of models to image-guided surgical interventions. Methods have been proposed for brain,[10–18] liver,[19–22] and for general organ deformation strategies.[23,24] Carter *et al.*[25] provide a review of mathematical modeling for image-guided surgery. Intraoperative validation of these models, in the absence of an intraoperative MRI or CT unit, is an open problem. We propose using a low-cost surface acquisition method that relies on the principle of conoscopic holography for model validation.

2. COMPENSATING FOR DEFORMATION WITH MATHEMATICAL MODELS

In this section, we give an overview of our specific framework for compensation of deformation in the brain using mathematical models. Note that the topic of this paper is validation of the framework; the framework itself has been described in other work (see for example, Chen *et al.*[8] and Dumpuri *et al.*[14,15]) and only described here for context. An illustration of the steps in our framework is provided in Figure 1. The preoperative and intraoperative steps are:
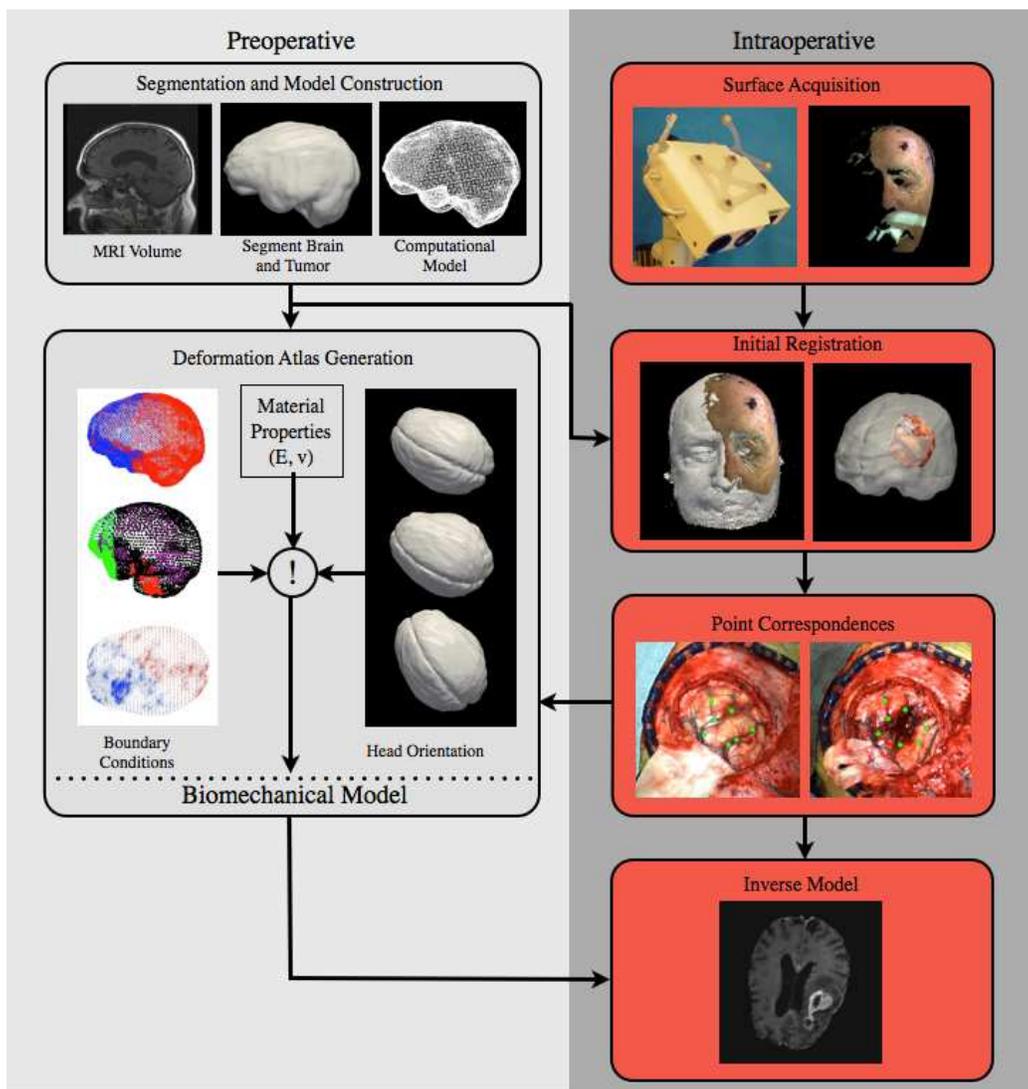
Preoperative

Segmentation and Model Construction

MRI Volume   Segment Brain and Tumor   Computational Model

Deformation Atlas Generation

Material Properties (E, v)

!

Boundary Conditions   Head Orientation

Biomechanical Model

Intraoperative

Surface Acquisition

Initial Registration

Point Correspondences

Inverse Model

Figure 1. Deformation correction framework used in study.

Preoperative Phase

1. **Patient Imaging.** A magnetic resonance image (MRI) volume is acquired using a 1.5T scanner, a similar scan is required in conventional surgery that uses image guidance. The MR volumes are T1 weighted and gadolinium enhanced with a voxel size of 1 mm × 1 mm × 1.2 mm.

2. **Segmentation of brain and tumor.** The brain is segmented from neighboring structures using an automatic method.[26] Manual refinements of the segmentation are typically required in the area of the tumor. The tumor is extracted using manual segmentation. A 3D surface model is constructed of both the brain and tumor using the marching cubes algorithm.[27] A 3D surface of the patient's head is extracted from the MR volume using marching cubes.

3. **Mesh construction.** The 3D surface model is smoothed and parameterized using the FastRBF toolkit (FarField Technology, Christchurch, NZ). Using the 3D surface model, a volumetric tetrahedral mesh is generated for use in our finite element model.[28]

4. **Atlas generation and boundary condition determination.** In our terminology, an atlas consists of a collection of possible deformations predicted by our model. The deformations represented in our atlas include: permeability (caused by mannitol, a hyperosmotic drug administered to reduce intracranial pressure), gravity (determined by the head orientation of the patient in the OR and the amount of cerebrospinal fluid leakage in the procedure), and swelling (caused by a physiological response). For these deformations, there are three types of boundary conditions: fixed (for the areas in proximity to the brain stem that undergo little deformation), stress free (region around and containing the craniotomy that is free to deform), and slippage (all other boundaries of the head can only move in the tangential direction, falx and tentoria). Grey and white matter elements are assigned their own material property. The tumor region is assigned another material property. Tissue resection is simulated by decoupling nodes belonging to the tumor material type. Once a complete set of boundary conditions is known, the computational model can be run and a volumetric prediction of organ deformation generated. We have found these techniques improve our ability to model deformation but further refinement is needed.

Intraoperative Phase

1. **Initial registration.** A laser range scan (Pathfinder Therapeutics Inc., Nashville, TN) of the patient's face is acquired prior to sterile field assembly. The scanner collects 3D surface data as a point cloud and a 2D texture of the scanned object. The surface is registered using the iterative closest point algorithm[29] to the 3D model of the patient's head that was extracted from the preoperative MR volume. This step provides the initial physical to image space transformation. All subsequent LRS acquisitions are in this space.

2. **Point correspondences.** An LRS surface is acquired after the dura is opened and prior to tumor resection, the tumor is resected, an LRS surface is acquired after resection. The LRS point cloud is fit with a high resolution surface using the FastRBF toolkit. Corresponding points are designated on the pre and post-resection bitmap image from the LRS acquisition. The corresponding 3D point is determined using the LRS point cloud and the FastRBF toolkit.

3. **Inverse model** The inverse model is solved using the atlas predictions built prior to surgery, driven by the homologous points picked in the last step. Simply stated, an inverse solution is obtained by the minimization of least-squared error between the predictions and the measured displacements. The details of this calculation can be found in Chen *et al.*[8] The displacement field calculated by the inverse model is used to deform the preoperative MR volume for updating the guidance display.

3. CONOSCOPIC HOLOGRAPHY

Conoscopic holography is a distance measurement method proposed by Sirat and Psaltis[30] traditionally used in industrial quality control. The technique relies on analyzing constructive and destructive interference patterns between emitted and reflected laser light. A method of optically tracking the device for non-contact surface characterization was developed at Vanderbilt University that can be deployed through a laparoscopic port.[31] The conoscopic holography sensor (Conoprobe Mark 3, Optimet Metrology Ltd., Jerusalem, Israel) was outfit with tracking targets. The conoprobe reports the distance

and direction from the laser source to the object being scanned. A calibration procedure establishes the transformation of the collected conoprobe points into the coordinate frame of the optical tracking system. In an accuracy test, the RMS error for the tracked conoprobe was found to be 0.77 mm.[32]

4. METHODS

In this study, we investigate the use of conoscopic holography for the characterization of a resection cavity for validation of mathematical models *in vivo*.

4.1 Apparatus

An optical tracking system (Polaris Spectra, Northern Digital Inc., Waterloo, ON, Canada) measured the position and orientation of all instruments and acquisition devices in the operating room (OR). An optically-tracked LRS (Pathfinder Therapeutics Inc., Nashville, TN, USA), conoprobe (Conoprobe Mark 3, Optimet Metrology Ltd., Jerusalem, Israel), and surgical instrument (Medtronic, Minneapolis, MN, USA) acquired intraoperative data. An optical tracking target (Medtronic) was attached to the patient. All data acquisitions were performed in the coordinate frame of the patient such that all data would be in a common coordinate frame. Figure 2 demonstrates the conoprobe in use in the OR for this study. The conoprobe was not sterilized since it was operated at a distance from the patient.

Figure 2. Conoprobe surface acquisition of patient undergoing resection surgery at Vanderbilt University Medical Center (Nashville, TN, USA). The single laser point is visible on the surface of the brain and the optical tracking target can be seen on the conoprobe.

4.1.1 Patient Selection

We acquired preoperative and intraoperative data for two patients. The first patient was a 37 year old-female with a low grade tumor in the left frontal lobe that required a small, approximately 2.5 cm craniotomy. The second patient was an 83 year-old male with a metastic tumor in the left frontal lobe that required a large, approximately 11.5 cm craniotomy. Patient consent was obtained prior to surgery for enrollment in the study as required by the Vanderbilt Institutional Review Board.

4.2 Data Acquisition and Processing

We acquired and processed data as outlined in Section 2 and detailed in Figure 1. In short, MR tomograms were acquired, the surface of the brain and tumor were segmented, and modeling data built, all preoperatively. In the operating room, an LRS of the patient's face, prior to sterile field assembly, was performed in order to establish initial correspondence from the coordinate frame of the LRS to the coordinate frame of the MR. Conoprobe*, LRS, and surgical instrument swabbing

---

*Due to technical issues, we were unable to acquire pre-resection surface data with the conoprobe in one case.
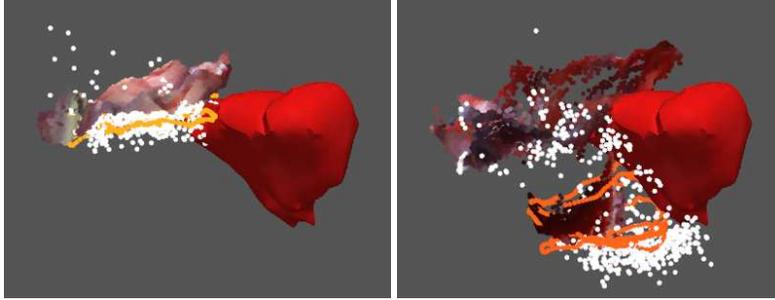
Figure 3. Pre- (left image) and post-resection (right image) data for case 1 is shown. Conoprobe (white), instrument swabbing (orange), and LRS is rendered with the segmented tumor (red). In this case, the intraoperatively acquired point clouds are shifted in the direction of gravity. Good agreement of the acquired points is observed in both the pre- and post-resection data sets. Note that in this case, the SNR of the conoprobe points was not acquired; hence, the conoprobe points are unprocessed.

data sets were acquired of the brain surface after opening the dura (and prior to resection) and after tumor resection. All data were transformed into the preoperative MR frame using the LRS to MR transformation computed using the LRS of the patient's face. Homologous points were identified in the pre- and post-resection LRS bitmap and used to drive our inverse model.

4.3 Evaluation

The accuracy of conoscopic holography techniques is affected by the absorption properties of the tissue under interrogation. The conoprobe software reports the signal-to-noise ratio (SNR) as a percentage for every point collection. The manufacturer of the device suggests only using points with an SNR greater than 30%. We did not record the SNR in the first data set acquired for this study. The noisy points in this collection prompted us to contact the manufacturer for advice on data collection. In the second data set, only points with SNR greater than 30% were used in our analysis.

We evaluated the accuracy of the model prediction using the intraoperatively collected conoprobe points and the model-predicted (deformed) tumor mesh. Using the tumor mesh (step 3 of the preoperative phase in Section 2) and the calculated deformation field from our inverse model (step 3 of the intraoperative phase in Section 2), a deformed tumor mesh was generated. For each point in the conoprobe collection, the nearest neighbor on the model-predicted tumor mesh was calculated. For comparison, for each point in the conoprobe collection, the nearest neighbor on the undeformed tumor mesh was calculated.

5. RESULTS

The pre- and post-resection data for all acquisition methods for case 1 and 2 are rendered in Figure 3 and Figure 4, respectively. In these figures, the conoprobe points are shown in white, the instrument swabbed points in orange, the LRS, and the tumor in red (segmented from preoperative scans).

The distance from the tumor surface to the conoprobe points with and without correction computed using nearest neighbors are summarized in Table 1. The conoprobe collections are rendered in Figures 5 and 6 with their associated distances.

Table 1. Distance from Tumor Surface to Conoprobe Points With and Without Correction

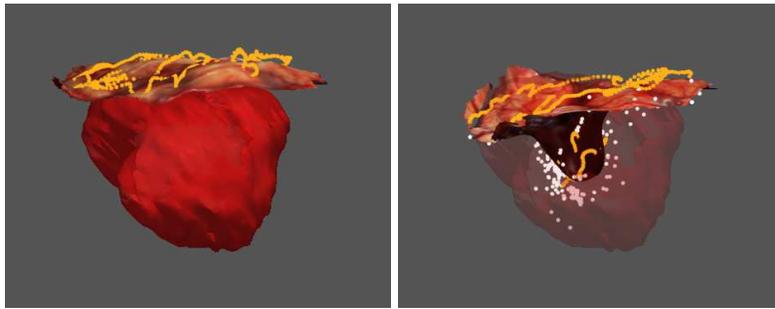| | | Distance (mm) | | | |
		mean	sdev	min	max
case 1	no correction	5.47	2.64	0.02	12.77
	correction	3.92	2.14	0.02	9.56
case 2	no correction	7.76	2.44	0.09	14.61
	correction	2.00	1.65	0.00	7.19

Figure 4. Pre- (left image) and post-resection (right image) data for case 2 is shown. Conoprobe (white), instrument swabbing (orange), and LRS is rendered with the segmented tumor (red). In this case, the large tumor caused the resection cavity to collapse thus making the cavity appear smaller than the tumor in its preoperative state. Good agreement of the acquired points is observed in both the pre- and post-resection data sets.
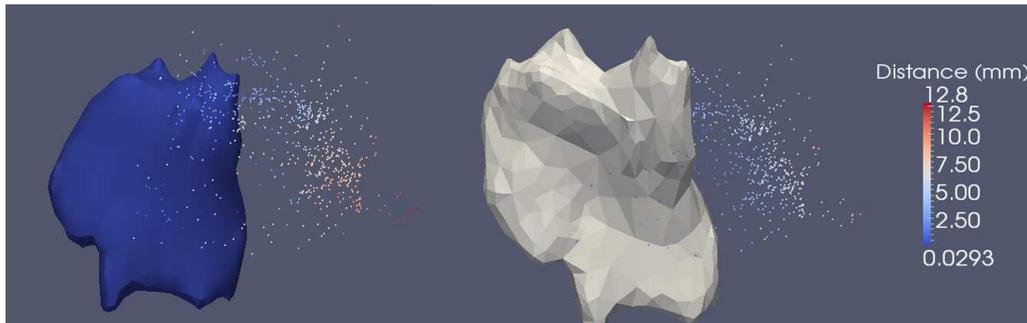

Figure 5. Tumor mesh (blue) with and (white) without deformation correction for case 1. Conoprobe points are rendered with their associated distances from the tumor surface.
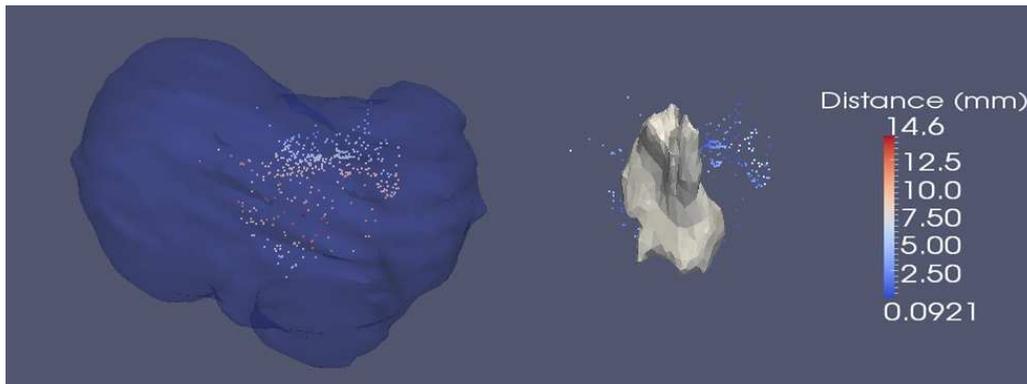

Figure 6. Tumor mesh (blue) with and (white) without deformation correction for case 2. Conoprobe points are rendered with their associated distances from the tumor surface.

6. DISCUSSION

In Figures 3 and 4, the displacement of the point clouds from the tumor represents the brain shift that occurred from the preoperative image state to the intraoperative state. For example, the point clouds in Figure 3 are shifted in the direction of gravity; hence, the lack of overlap of the points clouds and tumor. In case 2, the preoperative tumor appears significantly larger than the resection cavity acquired *in vivo* due to the collapsing of the cavity after resection. The same effect is not observed in case 1 because of the small tumor and craniotomy size relative to case 2.

In the post-resection comparison of the acquisition methods in Figure 3, the LRS does not sufficiently describe the full resection cavity due to the line-of-sight issue described earlier but the instrument and conoprobe swabbing largely overlap. In theory, one could obtain multiple scans of the cavity and reconstruct the full cavity from multiple scans; however, each scan requires a minute or so to acquire thus increasing operative time.

Note that in case 2, in order to address the spread of conoprobe points in the bottom of the cavity observed in case 1, the signal-to-noise ratio (SNR) for each conoprobe point, provided by the hardware manufacturer's software, was recorded and points with an SNR below 50% were omitted. No other manipulation of the points was performed.

In both cases, the distances from the conoprobe points to the tumor surface were significantly improved after correction. Case 2 appears to be a better correction than case 1; however, this is difficult to conclude with the noisy points from case 1 due to the SNR issue describes above.

7. CONCLUSIONS

The results suggest that the use of intraoperative conoscopic holography for tumor resection cavity characterization with the goal of intraoperative validation of deformation correction using mathematical models is promising. Additional patient data collection and evaluation is underway.

REFERENCES

[1] Nabavi, A., Black, P. M., Gering, D. T., Westin, C. F., Mehta, V., Pergolizzi, R. S., Ferrant, M., Warfield, S. K., Hata, N., Schwartz, R. B., Wells, W. M., Kikinis, R., and Jolesz, F. A., "Serial intraoperative magnetic resonance imaging of brain shift," *Neurosurgery* **48**(4), 787–797 (2001).

[2] Nimsky, C., Ganslandt, O., Cerny, S., Hastreiter, P., Greiner, G., and Fahlbusch, R., "Quantification of, visualization of, and compensation for brain shift using intraoperative magnetic resonance imaging," *Neurosurgery* **47**(5), 1070–1079 (2000).

[3] Roberts, D. W., Hartov, A., Kennedy, F. E., Miga, M. I., and Paulsen, K. D., "Intraoperative brain shift and deformation: A quantitative analysis of cortical displacement in 28 cases," *Neurosurgery* **43**(4), 749–758 (1998).

[4] Hartkens, T., Hill, D., Castellano-Smith, A., Hawkes, D., Maurer, C.R., J., Martin, A., Hall, W., Liu, H., and Truwit, C., "Measurement and analysis of brain deformation during neurosurgery," *IEEE Transactions on Medical Imaging* **22**(1), 82–92 (2003).

[5] Archip, N., Clatz, O., Whalen, S., Kacher, D., Fedorov, A., Kot, A., Chrisocholdes, N., Jolesz, F., Golby, A., Black, P. M., and Warfield, S. K., "Non-rigid alignment of pre-operative MRI, fMRI, and DT-MRI with intra-operative MRI for enhanced visualization and navigation in image-guided neurosurgery," *NeuroImage* **35**, 609–624 (April 2007).

[6] Black, P., Moriarty, T., Alexander, E., Stieg, P., Woodard, E., Gleason, P., Martin, C., Kikinis, R., Schwartz, R., and Jolesz, F., "Development and implementation of intraoperative magnetic resonance imaging and its neurosurgical applications," *Neurosurgery* **41**(4), 831–842 (1997).

[7] Letteboer, M., Willems, P., Viergever, M., and Niessen, W., "Brain shift estimation in image-guided neurosurgery using 3-D ultrasound," *IEEE Transactions on Biomedical Engineering* **52**(2), 268–276 (2005).

[8] Chen, I., Coffey, A. M., Ding, S. Y., Dumpuri, P., Dawant, B. M., Thompson, R. C., and Miga, M. I., "Intraoperative brain shift compensation: Accounting for dural septa," *IEEE Transactions on Biomedical Engineering* **58**, 499–508 (2011).

[9] Clatz, O., Delingette, H., Talos, I. F., Golby, A. J., Kikinis, R., Jolesz, F. A., Ayache, N., and Warfield, S. K., "Robust nonrigid registration to capture brain shift from intraoperative MRI," *IEEE Transactions on Medical Imaging* **24**, 1417–1427 (November 2005).

[10] Miller, K., "Constitutive model of brain tissue suitable for finite element analysis of surgical procedures," *Journal of Biomechanics* **32**, 531–537 (1999).

[11] Roberts, D. W., Miga, M., Hartov, A., Eisner, S., Lemery, J., Kennedy, F., and Paulsen, K., "Intraoperatively updated neuroimaging using brain modeling and sparse data," *Neurosurgery* **45**(5), 1199–1206 (1999).

[12] Vigneron, L. M., Warfield, S. K., Robe, P. A., and Verly, J. G., "3D XFEM-based modeling of retraction for preoperative image update," *Computer Aided Surgery* **16**, 121–134 (2011).

[13] Cash, D. M., Miga, M. I., Sinha, T. K., Galloway, R. L., and Chapman, W. C., "Compensating for intra-operative soft tissue deformations using incomplete surface data and finite elements," *IEEE Transactions on Medical Imaging* **24**, 1479–1491 (2005).

[14] Dumpuri, P., Thompson, R. C., Dawant, B. M., Cao, A., and Miga, M. I., "An atlas-based method to compensate for brain shift: Preliminary results," *Medical Image Analysis* **11**(2), 128–145 (2007).

[15] Dumpuri, P., Thompson, R. C., Cao, A. Z., Ding, S. Y., Garg, I., Dawant, B. M., and Miga, M. I., "A fast and efficient method to compensate for brain shift for tumor resection therapies measured between preoperative and postoperative tomograms," *IEEE Transactions on Biomedical Engineering* **57**, 1285–1296 (2010).

[16] Lunn, K. E., Paulsen, K. D., Lynch, D. R., Roberts, D. W., Kennedy, F. E., and Hartov, A., "Assimilating intraoperative data with brain shift modeling using the adjoint equations," *Medical Image Analysis* **9**(3), 281–293 (2005).

[17] Lunn, K. E., Paulsen, K. D., Liu, F. H., Kennedy, F. E., Hartov, A., and Roberts, D. W., "Data-guided brain deformation modeling: Evaluation of a 3-D adjoint inversion method in porcine studies," *IEEE Transactions on Biomedical Engineering* **53**, 1893–1900 (2006).

[18] Miga, M. I., Roberts, D. W., Kennedy, F. E., Platenik, L. A., Hartov, A., Lunn, K. E., and Paulsen, K. D., "Modeling of retraction and resection for intraoperative updating of images during surgery," *Neurosurgery* **49**, 75–85 (2001).

[19] Blackall, J., King, A., Penney, G., Adam, A., and Hawkes, D., "A statistical model of respiratory motion and deformation of the liver," in [*Medical Image Computing and Computer-Assisted Intervention MICCAI 2001*], Niessen, W. and Viergever, M., eds., *Lecture Notes in Computer Science* **2208**, 1338–1340, Springer Berlin / Heidelberg (2001).

[20] Blackall, J., Penney, G., King, A., and Hawkes, D., "Alignment of sparse freehand 3-D ultrasound with preoperative images of the liver using models of respiratory motion and deformation," *Medical Imaging, IEEE Transactions on* **24**(11), 1405–1416 (2005).

[21] Clements, L. W., Dumpuri, P., Chapman, R. L., R. L. Galloway Jr, and Miga, M. I., "Atlas-based method for model updating in image-guided liver surgery," in [*Medical Imaging 2007: Visualization, Image-Guided Procedures, and Modeling*], Cleary, K. R. and Miga, M. I., eds., **6509**, SPIE (2007).

[22] Dumpuri, P., Clements, L. W., Dawant, B. M., , and Miga, M. I., "Model-updated image-guided liver surgery: Preliminary results using surface characterization," *Progress in Biophysics and Molecular Biology* **103**(2-3), 197–207 (2010).

[23] Davatzikos, C., Shen, D. G., Mohamed, A., and Kyriacou, S. K., "A framework for predictive modeling of anatomical deformations," *IEEE Transactions on Medical Imaging* **20**, 836–843 (2001).

[24] Zhong, H. and Peters, T., "A real time hyperelastic tissue model," *Computer Methods in Biomechanics and Biomedical Engineering* **10**, 185–193 (2007).

[25] Carter, T. J., Sermesant, M., Cash, D. M., Barratt, D. C., Tanner, C., and Hawkes, D. J., "Application of soft tissue modelling to image-guided surgery," *Medical Engineering and Physics* **27**(10), 893–909 (2005). Advances in the finite element modelling of soft tissue deformation.

[26] Rohde, G., Aldroubi, A., and Dawant, B., "The adaptive bases algorithm for intensity-based nonrigid image registration," *IEEE Transactions on Medical Imaging* **22**, 1470–1479 (nov. 2003).

[27] Lorensen, W. E. and Cline, H. E., "Marching cubes: A high resolution 3D surface construction algorithm," in [*Proceedings of the 14th annual conference on Computer graphics and interactive techniques*], *SIGGRAPH '87*, 163–169, ACM, New York, NY, USA (1987).

[28] Sullivan, J. M., Charron, G., and Paulsen, K. D., "A three-dimensional mesh generator for arbitrary multiple material domains," *Finite Elements in Analysis and Design* **25**(3-4), 219–241 (1997).

[29] Besl, P. and McKay, N., "A method for registration of 3-D shapes," *IEEE Transactions on Pattern Analysis and Machine Intelligence* **14**(2), 239–256 (1992).

[30] Sirat, G. and Psaltis, D., "Conoscopic holography," *Optics Letters* **10**(1), 4–6 (1985).

[31] Lathrop, R. A., Hackworth, D. M., and Webster, R. J., "Minimally invasive holographic surface scanning for soft-tissue image registration," *IEEE Transactions on Biomedical Engineering* **57**(6), 1497–1506 (2010).

[32] Burgner, J., Simpson, A. L., Fitzpatrick, J. M., Lathrop, R. A., Herrell, S. D., Miga, M. I., and Webster III, R. J., "Image registration using conoscopic holography for minimally invasive surgery: Accuracy analysis and ex vivo human tissue experiments," *Submitted to International Journal of Medical Robotics and Computer Assisted Surgery* **-**, – (2012).